ChemComm

Chemical Communications

rsc.li/chemcomm

200 ℃

175 ℃   225 ℃

150 ℃   250 ℃

125 ℃   275 ℃

100 ℃

75 ℃

50 ℃   0 ℃

25 ℃

CO₂

ROYAL SOCIETY
OF CHEMISTRY

COMMUNICATION
Xu-Bing Li, Li-Zhu Wu *et al.*
Flower-like cobalt carbide for efficient carbon dioxide
conversion

Check for updates

Flower-like cobalt carbide for efficient carbon dioxide conversion†

Qing Guo,‡[ab] Shu-Guang Xia,‡[ab] Xu-Bing Li, ID *[ab] Yang Wang,[ab] Fei Liang, ID [bc] Zhe-Shuai Lin, ID [bc] Chen-Ho Tung ID [ab] and Li-Zhu Wu ID *[ab]

Catalytic conversion of carbon dioxide (CO_2) to value-added chemicals under mild conditions is highly desired, albeit with significant challenges. Here, in terms of exposure of abundant active sites and excellent photo-to-thermal conversion properties, flower-like Co_2C has been firstly used for effectively catalysing the cycloaddition of CO_2 with epoxides to produce cyclic carbonates with yields of up to 95% under solar light. Density functional theory (DFT) calculations reveal that Lewis acid sites of the surface Co atoms can activate both CO_2 and epoxide, thus opening up the possibility of a CO_2-epoxide cycloaddition reaction.

The increasing atmospheric concentration of carbon dioxide (CO_2), which is regarded as the main greenhouse gas, has caused serious environmental concerns (*e.g.*, global warming, abnormal climate change and sea level rise).[1–4] To address the anthropogenic CO_2 emission issues,[5–11] the approaches of physical CO_2 capture and storage,[12,13] and chemical conversion of CO_2 into usable fuels and/or value-added chemicals[14,15] have been widely investigated. From a chemical point of view, cycloaddition of CO_2 with epoxides represents one of the most promising strategies to generate valuable chemicals.[16–18] By using CO_2 as the renewable and nontoxic one-carbon (C_1) feedstock,[19] cyclic carbonates are produced with 100% atom-economy efficiency.[20] Cyclic carbonates can be directly employed in industry as solvents or intermediates, such as carbamates,[21] polycarbonates[22] and spiro compounds.[23] Numerous advances in homogeneous (*e.g.*, Co,[24,25] Ni,[26] Al[27] and Cu-based[28] monometallic or bimetallic complexes) and hetero-geneous (*e.g.*, metal–organic-frameworks (MOFs),[29–31] mesoporous polymers,[32] and zeolites[33]) catalysts have been made for the cycloaddition of CO_2 with epoxides. However, most of the state-of-the-art catalysts can work fairly well to yield cyclic carbonates only at an elevated temperature, thus leading to an increase of the energy cost.

Transition-metal carbides (TMCs) show great potential in the field of catalysis owing to their outstanding electronic conductivity, good chemical stability, abundant surface active sites and high photo-to-thermal conversion efficiency.[34–36] Cobalt carbide (Co_2C), for example, has been demonstrated to be an effective catalyst in various transformations (*e.g.*, hydrogen evolution and Fischer–Tropsch synthesis).[37,38] However, the application of cobalt carbide in cycloaddition of CO_2 with epoxides is still elusive. Considering these attributes, we are inspired to explore Co_2C as a novel catalyst for cycloaddition of CO_2 with epoxides by using solar energy to replace external thermal energy input for following reasons: (i) the high specific surface area and tuneable chemical composition provide abundant surface active sites to activate CO_2 and/or epoxides; (ii) the effective CO_2 adsorption ability on TMCs favours the very first step of CO_2 conversion;[39] (iii) the huge amount of heat released during the excellent photo-to-thermal conversion process would promote the endothermic reaction (high C=O bond energy of 750 kJ mol^{-1});[40] and (iv) the feasible separation and reusability of the hetero-geneous catalysts is beneficial for large-scale applications.[41] To our delight, flower-like Co_2C facilitates the catalysis of CO_2-epoxide cycloaddition with yields of up to ∼95% under visible light (Scheme 1), showing the first example of using TMCs for photothermal-driven CO_2 conversion.

Flower-like Co_2C was synthesized through a modified method of solution pyrolysis at high temperature (Fig. 1a),[42–44] see experimental details in the ESI.† Scanning electron microscopy (SEM) and transmission electron microscopy (TEM) clearly showed the flower-like morphology of the synthesized material (Fig. 1b and c). The average diameter of the nanoflowers was determined to be ∼500 nm by TEM characterization (Fig. 1c). The nearly apparent nanosheet on the outside of the nanoflowers indicated that the obtained nanoflower was a result of self-assembly of
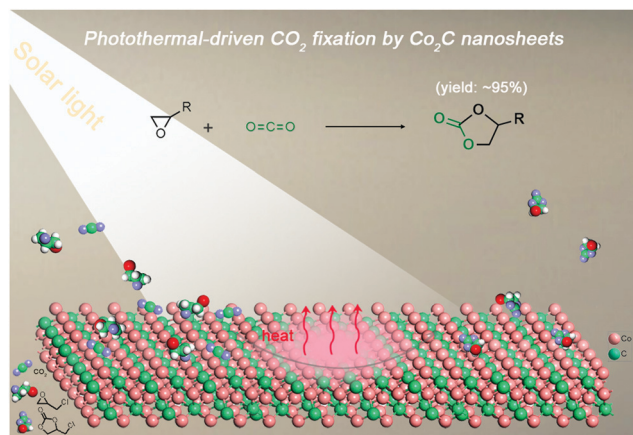
a Key Laboratory of Photochemical Conversion and Optoelectronic Materials, Technical Institute of Physics and Chemistry, Chinese Academy of Sciences, Beijing 100190, P. R. China. E-mail: lixubing@mail.ipc.ac.cn, lzwu@mail.ipc.ac.cn

b School of Future Technology, University of Chinese Academy of Sciences, Beijing 100049, P. R. China

c Key Laboratory of Functional Crystals and Laser Technology, Technical Institute of Physics and Chemistry, Chinese Academy of Sciences, Beijing 100190, P. R. China

Scheme 1 Illustration of the photothermal-driven cycloaddition of CO_2 with epoxides catalyzed by Co_2C nanosheets of the nanoflower.
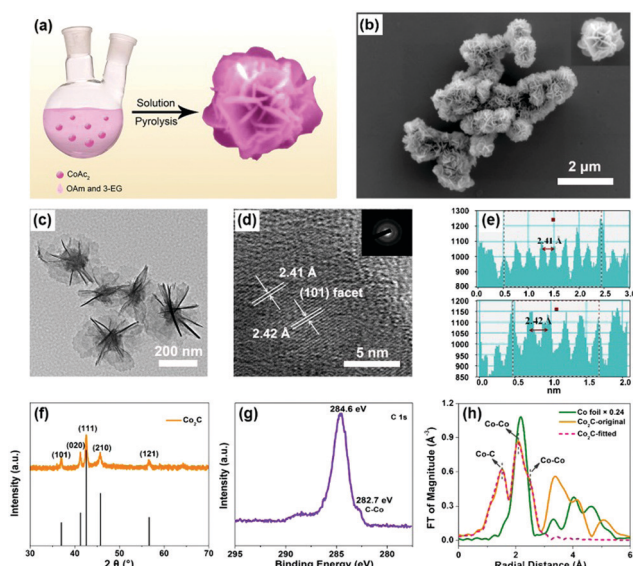

Fig. 1 (a) Synthetic process of flower-like Co_2C. (b) SEM image (the inset panel is the high-resolution SEM image) and (c) TEM image of Co_2C nanoflowers. (d) High-resolution TEM image of Co_2C (the inset panel is the corresponding SAED pattern). (e) The corresponding lattice distances of the exposed (101) plane of Co_2C. (f) XRD pattern and (g) C 1s XPS spectrum of Co_2C nanoflowers. (h) Magnitude of k^2-weighted Fourier transform of the Co K-edge EXAFS spectra of Co foil and the obtained Co_2C nanoflowers with corresponding curve-fitting results.

individual nanosheets. The thickness of individual nanosheet was determined to be ~2.4 nm by atomic force microscopy (AFM) (Fig. S1, ESI†). In the high-resolution TEM image, a lattice distance of ~2.41 Å was observed, indicating the exposure of the (101) facet of Co_2C (Fig. 1d and e). Moreover, selective area electron diffraction (SAED) patterns in Fig. 1d confirmed the polycrystalline nature of the synthesized materials. In addition, elemental mapping analysis indicated the coexistence of Co, C and O elements (Fig. S2, ESI†), which matched well with the X-ray photoelectron spectroscopy (XPS) results (see below).

The powder X-ray diffraction (XRD) (Fig. 1f) pattern of the as-prepared sample was in good agreement with the standard pattern of Co_2C (Joint Committee on Powder Diffraction Standards (JCPDS) Powder Diffraction File (PDF) No. 65-1457),[42] indicating the successful formation of Co_2C. The peaks at 1630, 1420 and 1050 cm^{-1} corresponding to C=C, C–H, and C–N bonds, respectively, in the Fourier transform infrared (FTIR) spectra (Fig. S3, ESI†) almost disappeared after calcination, suggesting the removal of surface organic ligands. Full XPS survey confirmed the coexistence of Co, C and O elements in the obtained sample (Fig. S4, ESI†). High-resolution XPS spectra of C 1s (Fig. 1g) and Co 2p (Fig. S5, ESI†) show the characteristic peaks of carbide and carbidic Co at 282.7 and 778.1 eV,[36,45,46] respectively. Combined with the peak at 531.6 eV in the O 1s XPS spectrum (Fig. S6, ESI†), the peak at 781.0 eV in the Co 2p XPS spectrum was attributed to the $Co(OH)_2$ species formed in the process of Co_2C preparation, proving the fact that solution pyrolysis under high temperature inevitably leads to the formation of trace amounts of the hydroxide impurity.[46,47] Fig. 1h shows the X-ray absorption spectra (XAS) of the obtained sample. The Co K-edge extended X-ray absorption fine structure (EXAFS) of the synthesized sample exhibits two peaks in the R-space, which could be assigned to the first Co–C shell (1.89 Å) and the second Co–Co shell (2.54 Å) of Co_2C, see the fitting details in Table S1, ESI†.

Then, photo-to-thermal conversion effects of Co_2C nanoflowers were experimentally examined. UV-vis-NIR diffuse reflectance spectroscopy (DRS) measurement indicated that the synthesized Co_2C nanoflowers showed strong absorption in the range of 300 to 1200 nm (Fig. S7, ESI†), directly confirming its excellent light-harvesting properties. When the water suspension of Co_2C nanoflowers (0.6 mg mL^{-1}) was exposed to a 635 nm laser at varied power densities (0.1, 0.5, 1.0 and 2.0 W cm^{-2}), the solution displayed apparent temperature elevation (Fig. 2a). For instance, under 635 nm laser irradiation (0.5 W cm^{-2}), the temperature of the Co_2C nanoflowers water suspension reached 42.8 °C in 13 minutes, while the temperature of pure water only increased to 24 °C under the same conditions (Fig. S8, ESI†). Huge amount of heat released from Co_2C nanoflowers was also monitored by an IR camera in the solid state. As shown in the inset panel of Fig. 2b, the local temperature of the powder Co_2C sample quickly increased to 116.8 °C upon exposure to a 635 nm laser (0.5 W cm^{-2}) for 4.0 min, further confirming the in situ conversion of solar light into heat.

On the basis of the time constant for heat transfer and the maximal steady-state temperature, photo-to-thermal conversion efficiency (η), regarded as a major parameter in evaluating the performance in converting light to heat of a given material,[48] of the flower-like Co_2C was calculated to be as high as ~63.1% at 635 nm (Fig. 2b and c, see details in the ESI†). The exceptional photo-to-thermal conversion performance of Co_2C nanoflowers obtained here was comparable with those of the reported materials (Table S2, ESI†). To further evaluate its photothermal stability, temperature variations of Co_2C nanoflowers suspension were recorded under light irradiation (laser on) followed by natural cooling to room temperature (laser off). As shown in Fig. 2d,
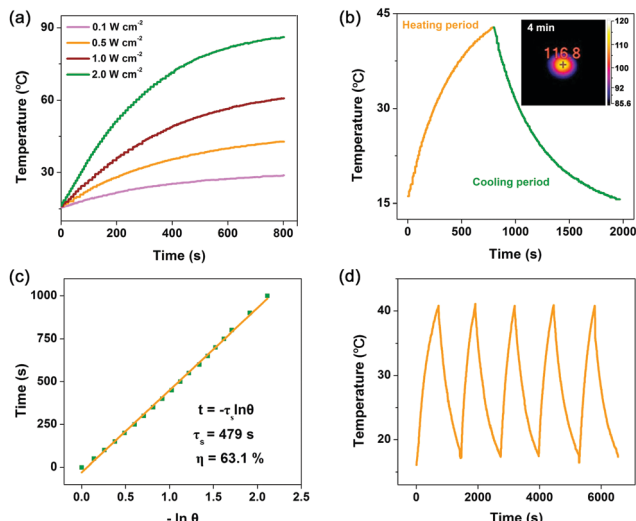
Fig. 2 (a) Photothermal heating curves of Co_2C nanoflowers dispersed in water under 635 nm laser irradiation at varied power densities (0.1, 0.5, 1.0 and 2.0 W cm^{-2}). (b) Photothermal effect of Co_2C aqueous dispersion under 635 nm laser irradiation (0.5 W cm^{-2}) and the cooling process after laser off. The inset panel in (b) is the IR image of Co_2C powder under 635 nm laser irradiation (0.5 W cm^{-2}) for 4.0 min. (c) The corresponding time constant (τ_s) for the heat transfer from the system determined by applying the linear time data from cooling period. (d) Recycling-heating curves of the Co_2C aqueous suspension with 635 nm laser irradiation at 0.5 W cm^{-2} for five laser on/off cycles.

negligible changes in temperature elevation were observed during 5 cycles, which highlighted the potential application of Co_2C nanoflowers as durable photothermal materials.

To investigate the catalytic performance of Co_2C nanoflowers, 3-chloropropylene oxide was chosen as the model substrate under visible light (Table 1). A water/fan-cooling system was employed to maintain the outside temperature of the reactor at room temperature, see experimental details in the ESI.† Increase of Co_2C nanoflowers from 0 to 25 mg obviously improved the yields up to ~93.5% (entries 1–4; Table 1). Control experiments showed that all components were essential for the conversion. Trace or negligible amount of the product was detected without light, tetrabutylammonium bromide (TBAB) or CO_2 (entries 5–7; Table 1). When tetrabutylammonium chloride (TBAC) was employed as the co-catalyst, a significantly declined yield of ~27% was observed (entry 8; Table 1). This result showed that easier dissociation and stronger nucleophilicity of Br^- compared to Cl^- dramatically benefited the ring-opening reaction of epoxides.[29] To verify the photothermal effects of Co_2C nanoflowers, we monitored the temperature variation of the reaction solution by using a thermometer. Upon light irradiation, the temperature of the solution was significantly elevated to ~60 °C in a period of 35 min (Fig. S9, ESI†), indicating the conversion of light into heat. Moreover, very similar yields were observed under either visible-light irradiation or external heating (60 °C), implying that the photothermal effects could promote the cycloaddition reaction between CO_2 and epoxide (Fig. S10, ESI†).

Furthermore, the obtained Co_2C sample was treated with hydrochloric acid (HCl; 6 mol L^{-1}) to exclude the contribution

Table 1 Optimization of the reaction conditions[a]

Entry	Catalyst	Additive	Yield[b] (%)
1	Co_2C (0 mg)	TBAB	< 5
2	Co_2C (15 mg)[c]	TBAB	54
3	Co_2C (15 mg)	TBAB	73.3
4	Co_2C (25 mg)	TBAB	93.5
5	Co_2C (25 mg)[d]	TBAB	< 5
6	Co_2C (25 mg)	—	0
7	Co_2C (25 mg)[e]	TBAB	0
8	Co_2C (15 mg)[f]	TBAC	26.7
9	Co_2C (25 mg)[g]	TBAB	81.9
10	$Co(OH)_2$ (25 mg)	TBAB	64
11	CoO (25 mg)	TBAB	63.6
12	Co_3O_4 (25 mg)	TBAB	48.6
13	Co_2C (50 mg)[h]	TBAB	66.4

[a] Reaction conditions: 0.15 mmol 3-chloropropylene oxide, 0.25 mmol TBAB, 3 mL CH_3CN as the solvent, blue LEDs (λ = 450 nm) as the light source, 15 h. [b] The carbonate product was quantified by ^1H NMR with diphenylmethanol as the internal standard. The yield was calculated by the equation, $[\eta\ (\%) = n(\text{carbonate})/n(3\text{-chloropropylene oxide}) \times 100\%]$. [c] 0.1 mmol TBAB. [d] No light irradiation. [e] N_2 instead of CO_2. [f] 0.1 mmol TBAC. [g] Co_2C nanoflowers treated with HCl (6 mol L^{-1}). [h] 0.50 mmol TBAB, AM 1.5 (100 mW cm^{-2}) as the light source, 24 h.

of trace amounts of cobalt hydroxide (i.e., $Co(OH)_2$) and/or cobalt oxide (i.e., CoO and Co_3O_4) on the surface of Co_2C nanoflowers in CO_2 fixation. After treating the sample with HCl, the slightly declined yield of the target product was still much higher than those of pure $Co(OH)_2$, CoO, or Co_3O_4 under the same conditions (entries 9–12; Table 1). These results confirmed that Co_2C, but not the hydroxide or oxide impurities, served as the real active sites for CO_2 fixation. More importantly, the Co_2C catalysed cycloaddition reaction of CO_2 and epoxides with electron-donating/withdrawing groups could also give rise to products in good to excellent yields (~95%) (Table S3, ESI†). Even under AM1.5 irradiation (entry 13; Table 1), this reaction proceeded with good yields. The activity was well preserved after three-time recycling (Fig. S11, ESI†), indicating the potential use of sunlight as the energy source for enhanced photothermal catalysis.

Based on the above experimental results, a plausible mechanism of the Co_2C nanoflowers catalysed CO_2-epoxide cycloaddition reaction is proposed (Fig. 3). Epoxide molecules adsorb on the surface exposed Co sites via Co–O interaction with an adsorption energy of −0.53 eV (Fig. S12a, see details of density functional theory (DFT) calculations in the ESI†), thereby
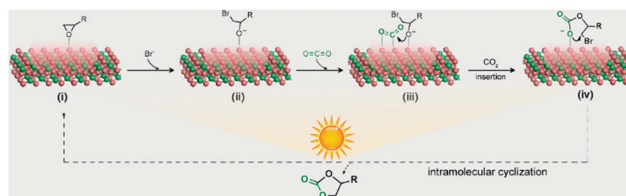

Fig. 3 The proposed mechanism of Co_2C catalysed CO_2 cycloaddition with epoxides under light irradiation.

leading to the elongation of C–O bond from 1.956 to 2.086 Å. Then, the nucleophilic Br⁻ ion attacks the adsorbed epoxide at the less hindered carbon atom to generate the metal alkoxide intermediate *via* the ring-opening reaction. At the same time, CO_2 adsorbs on the surface Co atom to give a bent molecular configuration (O1–C–O2 angle 146.99°) with a concerted interaction of C–Co and O–Co coordination (Fig. S12b, ESI†). With the aid of photothermal Co_2C nanoflowers, the oxygen anion of the alkoxide intermediate combines with the adjacent highly activated CO_2 molecules to yield the cyclic carbonate product, which is eventually released into the solvent to regenerate the catalyst. As a huge amount of heat is released due to the excellent photo-to-thermal conversion effects of Co_2C, the endothermic CO_2 cycloaddition reaction proceeds with high yields, which is comparable with the reported results (Table S4, ESI†).

In summary, an efficient CO_2 cycloaddition reaction with epoxides is achieved on low-priced photothermal catalyst of Co_2C nanoflowers. The yield of cyclic carbonates is up to ~95% with visible-light irradiation, owing to the excellent photothermal effects of Co_2C nanoflowers in converting light to heat. Besides, the high specific area as well as efficient CO_2 adsorption on the exposed Co atoms of the catalysts can simultaneously activate the adsorbed CO_2 and epoxides, thus promoting the CO_2 fixation reaction. This work provides new insights into the utilization of TMCs in the field of advanced photothermal-driven catalysis. Moreover, the influence of the morphology, size and thickness of TMCs on the catalytic performance will be further investigated by us.

Conflicts of interest

There are no conflicts to declare.

Notes and references

1 H.-L. Wu, X.-B. Li, C.-H. Tung and L.-Z. Wu, *Adv. Mater.*, 2019, **31**, 1900709.
2 X. Jiao, Z. Chen, X. Li, Y. Sun, S. Gao, W. Yan, C. Wang, Q. Zhang, Y. Lin, Y. Luo and Y. Xie, *J. Am. Chem. Soc.*, 2017, **139**, 7586–7594.
3 S. C. Peter, *ACS Energy Lett.*, 2018, **3**, 1557–1561.
4 J. Ran, M. Jaroniec and S.-Z. Qiao, *Adv. Mater.*, 2018, **30**, 1704649.
5 Q. Jiang, Z. Chen, J. Tong, M. Yang, Z. Jiang and C. Li, *Chem. Commun.*, 2017, **53**, 1188–1191.
6 S. Wang, B. Y. Guan and X. W. D. Lou, *J. Am. Chem. Soc.*, 2018, **140**, 5037–5040.
7 Y. Wang, Z. Zhang, L. Zhang, Z. Luo, J. Shen, H. Lin, J. Long, J. C. S. Wu, X. Fu, X. Wang and C. Li, *J. Am. Chem. Soc.*, 2018, **140**, 14595–14598.
8 X. Meng, S. Ouyang, T. Kako, P. Li, Q. Yu, T. Wang and J. Ye, *Chem. Commun.*, 2014, **50**, 11517–11519.
9 Q. Guo, F. Liang, X.-B. Li, Y.-J. Gao, M.-Y. Huang, Y. Wang, S.-G. Xia, X.-Y. Gao, Q.-C. Gan, Z.-S. Lin, C.-H. Tung and L.-Z. Wu, *Chem*, 2019, **5**, 2605–2616.
10 Y. Bai, J. Zhao, S. Feng, X. Liang and C. Wang, *Chem. Commun.*, 2019, **55**, 4651–4654.
11 J. C. Matsubu, V. N. Yang and P. Christopher, *J. Am. Chem. Soc.*, 2015, **137**, 3076–3084.
12 D. J. Heldebrant, P. K. Koech, V.-A. Glezakou, R. Rousseau, D. Malhotra and D. C. Cantu, *Chem. Rev.*, 2017, **117**, 9594–9624.
13 G. Kupgan, L. J. Abbott, K. E. Hart and C. M. Colina, *Chem. Rev.*, 2018, **118**, 5488–5538.
14 X.-B. Li, C.-H. Tung and L.-Z. Wu, *Angew. Chem., Int. Ed.*, 2019, **58**, 10804–10811.
15 C. Lu, J. Yang, S. Wei, S. Bi, Y. Xia, M. Chen, Y. Hou, M. Qiu, C. Yuan, Y. Su, F. Zhang, H. Liang and X. Zhuang, *Adv. Funct. Mater.*, 2019, **29**, 1806884.
16 F. Liu, K. Huang, Q. Wu and S. Dai, *Adv. Mater.*, 2017, **29**, 1700445.
17 M. Ding and H.-L. Jiang, *ACS Catal.*, 2018, **8**, 3194–3201.
18 M. Scharfenberg, J. Hilf and H. Frey, *Adv. Funct. Mater.*, 2018, **28**, 1704302.
19 T. Sakakura, J.-C. Choi and H. Yasuda, *Chem. Rev.*, 2007, **107**, 2365–2387.
20 Y. Fan, M. Tiffner, J. Schörgenhumer, R. Robiette, M. Waser and S. R. Kass, *J. Org. Chem.*, 2018, **83**, 9991–10000.
21 R. Zevenhoven, S. Eloneva and S. Teir, *Catal. Today*, 2006, **115**, 73–79.
22 D. J. Darensbourg, *Chem. Rev.*, 2007, **107**, 2388–2410.
23 Y.-X. Zhang, L. Guo, Y.-H. Wang, L.-L. Zhu and Z.-I. Chen, *Synth. React. Inorg., Met.-Org., Nano-Met. Chem.*, 2009, **39**, 445–448.
24 X.-B. Lu and D. J. Darensbourg, *Chem. Soc. Rev.*, 2012, **41**, 1462–1484.
25 X. Jiang, F. Gou, F. Chen and H. Jing, *Green Chem.*, 2016, **18**, 3567–3576.
26 J. Honores, D. Quezada, G. Chacón, O. Martínez-Ferraté and M. J. C. L. Isaacs, *Catal. Lett.*, 2019, **149**, 1825–1832.
27 C. J. Whiteoak, N. Kielland, V. Laserna, E. C. Escudero-Adán, E. Martin and A. W. Kleij, *J. Am. Chem. Soc.*, 2013, **135**, 1228–1231.
28 J. P. Hallett and T. Welton, *Chem. Rev.*, 2011, **111**, 3508–3576.
29 Q. Yang, C.-C. Yang, C.-H. Lin and H.-L. Jiang, *Angew. Chem., Int. Ed.*, 2019, **58**, 3511–3515.
30 H. He, J. A. Perman, G. Zhu and S. Ma, *Small*, 2016, **12**, 6309–6324.
31 P.-Z. Li, X.-J. Wang, J. Liu, J. S. Lim, R. Zou and Y. A. Zhao, *J. Am. Chem. Soc.*, 2016, **138**, 2142–2145.
32 G. Ji, Z. Yang, H. Zhang, Y. Zhao, B. Yu, Z. Ma and Z. Liu, *Angew. Chem., Int. Ed.*, 2016, **55**, 9685–9689.
33 D. Liu, G. Li, J. Liu, Y. Wei and H. Guo, *ACS Appl. Mater. Interfaces*, 2018, **10**, 22119–22129.
34 S. Cao, B. Shen, T. Tong, J. Fu and J. Yu, *Adv. Funct. Mater.*, 2018, **28**, 1800136.
35 Z. W. Seh, K. D. Fredrickson, B. Anasori, J. Kibsgaard, A. L. Strickler, M. R. Lukatskaya, Y. Gogotsi, T. F. Jaramillo and A. Vojvodic, *ACS Energy Lett.*, 2016, **1**, 589–594.
36 R. Zhao, M. Wang, D. Zhao, H. Li, C. Wang and L. Yin, *ACS Energy Lett.*, 2018, **3**, 132–140.
37 J. C. Mohandas, M. K. Gnanamani, G. Jacobs, W. Ma, Y. Ji, S. Khalid and B. H. Davis, *ACS Catal.*, 2011, **1**, 1581–1588.
38 Q. Guo, F. Liang, X.-Y. Gao, Q.-C. Gan, X.-B. Li, J. Li, Z.-S. Lin, C.-H. Tung and L.-Z. Wu, *ACS Catal.*, 2018, **8**, 5890–5895.
39 I. Persson, J. Halim, H. Lind, T. W. Hansen, J. B. Wagner, L. A. Naslund, V. Darakchieva, J. Palisaitis, J. Rosen and P. O. A. Persson, *Adv. Mater.*, 2019, **31**, 1805472.
40 J. Wu, Y. Huang, W. Ye and Y. Li, *Adv. Sci.*, 2017, **4**, 1700194.
41 J. Peng, J. Chen, W.-J. Ong, X. Zhao and N. Li, *Chem*, 2019, **5**, 18–50.
42 L. Zhong, F. Yu, Y. An, Y. Zhao, Y. Sun, Z. Li, T. Lin, Y. Lin, X. Qi, Y. Dai, L. Gu, J. Hu, S. Jin, Q. Shen and H. Wang, *Nature*, 2016, **538**, 84.
43 Z. J. Huba and E. E. Carpenter, *CrystEngComm*, 2014, **16**, 8000–8007.
44 M. Zamanpour, S. Bennett, P. Taheri, Y. Chen and V. G. Harris, *J. Appl. Phys.*, 2014, **115**, 17A747.
45 H. Wang, S. P. Wong, W. Y. Cheung, N. Ke, W. F. Lau, M. F. Chiah and X. X. Zhang, *Mater. Sci. Eng., C*, 2001, **16**, 147–151.
46 S. Li, C. Yang, Z. Yin, H. Yang, Y. Chen, L. Lin, M. Li, W. Li, G. Hu and D. Ma, *Nano Res.*, 2017, **10**, 1322–1328.
47 D. Gazzoli, M. Occhiuzzi, A. Cimino, D. Cordischi, G. Minelli and F. Pinzari, *J. Chem. Soc., Faraday Trans.*, 1996, **92**, 4567–4574.
48 L. Yuwen, J. Zhou, Y. Zhang, Q. Zhang, J. Shan, Z. Luo, L. Weng, Z. Teng and L. Wang, *Nanoscale*, 2016, **8**, 2720–2726.